이학석사학위논문

A mechanism for the ENSO amplitude modulation associated with the Atlantic Multi-decadal Oscillation

대서양 장주기 변동에 따른 ENSO 조절 메커니즘

2014년 2월

서울대학교 대학원

지구환경과학부

노 현 호

Abstract

A mechanism for the ENSO amplitude modulation associated with the Atlantic Multi-decadal Oscillation

Hyun-Ho No

School of Earth and Environmental Sciences

The Graduate School

Seoul National University

The modulation of the El Niño-Southern Oscillation (ENSO) amplitude caused by the Atlantic Multi-decadal Oscillation (AMO) is investigated in this study by using observational data and a Coupled General Circulation Model (CGCM). The observational data for the period 1900-2013 show that the ENSO variability weakened during the positive phase of the AMO and strengthened in the negative phase. In particular, the weakening of the ENSO amplitude for the past 15 years is related to changes in the Pacific mean climate: e.g., the SST cooling in the eastern Pacific and the easterly wind anomalies in the equatorial central Pacific. The observed changes were reproduced reasonably well by

CGCM simulations that were performed with the Atlantic Ocean SST nudged perpetually with the observed SST representing the positive phase of the AMO and free integration in the other oceans. Using a hybrid coupled model, it was determined that the mechanism associated with the weakening of the ENSO amplitude is related to the westward shift of the ENSO zonal wind stress anomalies in the positive phase of the AMO. This westward shift of the zonal wind stress anomalies results from the westward shift of precipitation anomalies associated with the relatively cold background mean SST over the central Pacific in the positive phase of the AMO. Thus, the present study demonstrates that the AMO plays an important role in modulating the amplitude of ENSO through mean state changes over the tropical Pacific.

Keywords: Westward shift of zonal wind stress, AMO, ENSO, Climate shift, natural variability, CGCM

Student number: 2012-20338

Contents

List of table and figures

1. Introduction

The north Atlantic Ocean sea surface temperature (SST) exhibits a multi-decadal variability called the Atlantic Multi-decadal Oscillation (AMO), which has been described by observational and modeling studies (Kerr 2000; Delworth and Mann 2000; Knight et al. 2005). Many studies have suggested that the multi-decadal SST variability over the north Atlantic is linked to a strengthening of the Atlantic Meridional Overturning Circulation (AMOC), which has a distinctive thermohaline circulation with multi-decadal time scales (Delworth and Mann 2000; Knight et al. 2005; Zhang et al. 2007; Wang et al. 2010). A positive phase of the AMO occurred after 1995 and was accompanied by SST warming over the northern Atlantic. Simultaneously, the El Niño-Southern Oscillation (ENSO) variability exhibited a weakening over the tropical Pacific. However, a detailed analysis of the relationship between the AMO and the ENSO variability is still lacking. This study is aimed to investigate the mechanisms related to the ENSO amplitude modulation associated with the AMO.

The linkage between the variability of the Atlantic SST and ENSO through an atmospheric bridge has been suggested by observational studies and coupled GCM (CGCM) experiments (Dong et al. 2006; Timmermann et al. 2007; Dong

and Sutton 2007; Rodriguez-Fonseca et al. 2009; Kayano and Capistrano 2013; Keenlyside et al. 2013). Ding et al. (2012) showed that SST warming over the equatorial Atlantic strengthens the Walker circulation over the tropical Pacific, which subsequently produces strong easterly wind anomalies over the central Pacific after several months. On multi-decadal timescales, Dong et al. (2006) showed that weak ENSO variability was associated with the positive phase (and vice versa) of the AMO using coupled GCM simulations with relaxing SSTs over the Atlantic Ocean. They suggested that the easterly wind anomalies in the central Pacific associated with the positive phase of the AMO contributed to reduced ENSO variability with shallower thermocline heights in the eastern Pacific (Dong et al. 2006; Rodriguez-Fonseca et al. 2009). However, the reason for weaker ENSO variability resulting from shallower mean thermocline heights is unclear, but the shallower mean thermocline heights in the eastern Pacific may amplify the ENSO amplitude because of more effective SST changes with the same upwelling.

The Pacific climatological-mean climate, particularly SSTs, has been known to influence the ENSO amplitude (An and Wang 2000; Yeh and Kirtman 2005; Kim et al. 2011; Xiang et al. 2013; Chung and Li 2013). Recently, Chung and Li (2013) demonstrated that the modulation of the ENSO amplitude is associated

with decadal changes in the mean SST over the tropical Pacific, particularly through changes in the east-west gradient of the tropical Pacific SSTs and associated precipitation distributions. By using coupled model experiments with different parameter values for the convection scheme, Kim et al. (2011) showed that the ENSO amplitude is sensitive to the mean precipitation over the eastern Pacific: increased mean precipitation over the eastern Pacific results in an increase in the ENSO amplitude. In that study, the increased mean precipitation over the eastern Pacific induced an eastward shift of the ENSO atmospheric component, which then resulted in stronger ENSO variability. Although those studies suggested that the changes in the mean SST and precipitation in the tropical Pacific can modify the ENSO amplitude through a zonal shift of ENSO atmospheric components, the mechanism underlying this phenomenon is unclear at present. The zonal wind stress anomalies associated with ENSO could be shifting in association with the zonal shifts in mean climate in the tropical Pacific, which would support the findings of Kang and Kug (2002), who suggested that the zonal shift in zonal wind stress anomalies associated with ENSO results in the change in the ENSO amplitude.

The present study provides additional evidence for associating the modulation of the ENSO amplitude with the Atlantic SST anomalies related to

the AMO by using long-term observational data and a coupled GCM. We also investigated the mechanism related to the association of the ENSO amplitude with the AMO in terms of the changes (zonal displacement) in ENSO zonal wind stress anomalies in different phases of the AMO. Section 2 describes the data and models used. The changes in mean climate in the Pacific and the ENSO variability associated with changes in the AMO are presented in Section 3. The mechanism related to the changes in the ENSO amplitude is investigated in Section 4, and a summary and discussion are presented in Section 5.

2. Description of data and model

a. Observational data sets

The monthly mean SST data from January 1900 to May 2013 used in the present study were obtained from the National Oceanic and Atmospheric Administration (NOAA) Extended Reconstructed SST (ERSST V.3; Smith et al. 2008). The horizontal resolution of the SST data is 2° by 2° in longitude and latitude. The precipitation data for January 1979 to May 2013 were obtained from the Global Precipitation Climatology Project (GPCP, Adler et al. 2003). The horizontal resolution of the GPCP precipitation data is 2.5° by 2.5° in longitude and latitude. We also used the monthly mean 850 hPa zonal wind data from January 1948 to May 2013 obtained from the National Centers for Environmental Prediction (NCEP)/National Center for Atmospheric Research (NCAR) Reanalysis (Kalnay et al. 1996). The horizontal resolution of 850 hPa zonal wind data is 2.5° by 2.5° in longitude and latitude. Linear trends of all observational data were removed, and the average of the monthly mean data from June to May of next year was used as an annual mean.

b. Model description

The Coupled General Circulation Model (CGCM) used in this study is a

Seoul National University (SNU) CGCM (Kug et al. 2008; Kim et al. 2008; Ham et al. 2012). The atmospheric portion of the model (AGCM) has a spectral resolution of T42 and 20 vertical sigma levels. The physics of the model includes parameterizations of convections, radiation, planetary boundary layers (PBL), and land surfaces. The deep convection scheme is a simplified Arakawa-Schubert scheme (Numaguti et al. 1995), the boundary layer scheme is a nonlocal diffusion scheme described by Holtslag and Boville (1993), and the radiation processes are parameterized by the two-stream k-distribution scheme implemented by Nakajima et al. (1995). The land surface processes are represented by the land surface model of Bonan (1996), which was developed at the National Center for Atmospheric Research. A detailed description of physical parameterizations in the AGCM can be found in Lee et al. (2001, 2003). The oceanic portion of the model is the Modular Ocean Model version 2.2 (MOM 2.2) developed at the Geophysical Fluid Dynamics Laboratory of Princeton University. The zonal resolution is 1° and the meridional resolution is 1/3° between 8°S and 8°N, gradually increasing to 3° in the extratropics. The vertical levels are configured with 23 levels in the upper 450 m and with a 10 m thickness of the top 10 layers. The mixed layer ocean model (Noh and Kim 1999) is embedded in the present ocean model. The air-sea coupling interval of the

coupled model is 2 hours (Ham et al. 2012). No flux correction is applied, and the model does not show significant climate drift in free long-term integrations.

Another model used in this study is a hybrid coupled model (Kang and Kug 2000). The oceanic component of the model is based on an intermediate ocean model similar to the Cane-Zebiak (CZ) ocean model (Cane and Zebiak 1987). The present model differs from the CZ model by a modification of the subsurface temperature formula. The formula used in the present model is based on a statistical relationship between the subsurface temperature and thermocline height, which was obtained from the NCEP ocean assimilation data. The atmospheric component of the hybrid coupled model provides the wind stress anomalies to force the ocean model, which are computed as a function of model Nino 3 SST anomalies. Details of the model can be obtained in Kang and Kug (2000, 2002).

3. Changes of mean climate in the Pacific and the ENSO variability associated with the AMO

The changes in the Pacific mean climate and the ENSO amplitude associated with the Atlantic SST anomalies related to the AMO were analyzed with long-term observational data, and the changes were then reproduced with the CGCM. The multi-decadal SST variability over the north Atlantic is linked to the strengthening of the AMOC (Delworth and Mann 2000; Knight et al. 2005; Zhang et al. 2007; Wang et al. 2010). A strengthened AMOC leads to large meridional heat transport from the equator to high latitudes and causes SST warming over the whole northern Atlantic. In the present study, we defined the AMO index as the 121-month running mean of the detrended SST anomalies averaged over the north Atlantic region (70°W - 0°W, 0°N - 60°N) (Knight et al. 2005; Sutton and Hodson 2005). The AMO index, obtained by applying a 121-month running mean, does not show the AMO state for the first year and the most recent 5 years. The monthly index without the smoothing is presented. Fig. 1 shows the AMO index (shaded) and the monthly index (solid line) and indicates that the positive phase of the AMO has been occurring recently. Consecutive 15-year periods were chosen to define the positive and negative

phases of the AMO, with the periods 1930-1945 and 1998-2013 defining the positive phases and those of 1904-1919 and 1979-1994 defining the negative phases. Fig. 2 shows the global distribution of the SST differences between the average values for the two positive phases and negative phases. The SST difference map shows that the SST anomalies typically occurred during the positive phase of the AMO, particularly over the Atlantic Ocean (Enfield et al. 2001; Knight et al. 2005), and the spatial pattern of the map is similar to that of the SST anomalies averaged for recent decades, as seen in Fig. 3. Because precipitation data are available after 1979, the difference maps of SST (Fig. 3a), precipitation (Fig. 3b), and 850 hPa zonal wind (Fig. 3c) between the two recent periods of 1998-2013 (the positive phase) and 1979-1994 (the negative phase) were calculated and are shown in Fig. 3. In the recent decade, the Atlantic SST showed a relatively large warming in the Northern Hemisphere and a large SST warming of the western extratropical Pacific in the Northern and Southern Hemisphere. However, a significant SST cooling has been located in the central Pacific. As will be discussed in the next section, this central Pacific SST change is a crucial factor for modulating the ENSO variability. Associated with the SST changes, notable changes in precipitation and lower-level wind occurred in the tropical Pacific. The most notable changes are the easterly wind anomalies in the

central equatorial Pacific and the dry and wet anomalies in the tropical central and western Pacific, respectively. The mechanism underlying the changes in SST, wind, and precipitation in the Pacific associated with the recent AMO is well-described in Hong et al. (2013).

The ENSO variability for different AMO phases was analyzed. Figs. 4a and 3c show the standard deviations of SST anomalies in the negative phases of the AMO for 1904-1919 and 1979-1994, respectively, and Figs. 4b and 4c show the standard deviations of SST anomalies in the positive phases of the AMO for 1930-1945 and 1998-2013, respectively. The SST variability in the positive phases of the AMO (Fig. 4b and 4d) is clearly weaker than the variability in the negative phases (Fig. 4a and 4c). In addition, the center of the SST anomaly moved to the central Pacific during the El Niño events in the recent decade, as shown by Xiang et al. (2013) and Chung and Li (2013).

We performed two CGCM experiments to investigate the extent to which the observed changes over the Pacific (as mentioned above) were associated with changes of the AMO (Table 1). In the first CGCM experiment, the Atlantic SST was nudged with the seasonally varying climatological SST obtained from a 100-year free run, wherein the other oceans run freely (hereafter, the CNT run). The second experiment was the same as the first except that the Atlantic SST

was nudged with the model climatological cycle and the observed SST anomalies, which represented the positive phase of the AMO (hereafter, the AMO run) as shown in Fig. 2. The nudging time scale used here was 1 day so that the simulated SST state in the Atlantic was kept more-or-less in a state of nudged SST. Both runs were integrated for 180 years and the model data produced for last 150 years were used in the present study.

Fig. 5 shows the mean state differences averaged for 150 years between the AMO run and the CNT run. As expected, the SST difference in the Atlantic Ocean is almost the same as the nudged SST anomaly, and a large SST warming is located in the western extratropical and in the northern Pacific. However, a significant SST cooling is also located in the central Pacific. Figs. 4b and 4c show the simulated differences of precipitation and 850 hPa zonal wind, respectively. The easterly wind anomalies appear in the central equatorial Pacific, and the dry and wet anomalies appear in the tropical central and western Pacific, respectively. The CGCM results are similar to those observed in Fig. 3, indicating that a large fraction of the observed mean changes in the Pacific for recent decades are related to the AMO.

The atmospheric responses associated with the positive phase of AMO over the Pacific have been analyzed in details with Gill-type response (Hong et al.

2013; Losada et al. 2010; Kucharski et al. 2011). The convectional Gill-type response indicates strong easterly anomalies in the east of heating as a Kelvin wave response (Gill 1980). In our model result, however, a strong easterly anomaly located in the central Pacific in which it is little far from the warming in Atlantic. Hong et al (2013) suggested that warming in the Atlantic induces strong easterly anomalies over the central Pacific not only as Gill-type response but also as feedback from the warm pool in the western Pacific. Apart from the warming in the Atlantic, warm pool in the western Pacific induces strong easterly anomalies in the central Pacific as the Gill-type response. Consequently, in the central Pacific, there are easterly anomalies caused by warming in the Atlantic and other easterly anomalies due to the response to warm pool. As combining these influences, strong easterly anomalies exist over the central Pacific (Hong et al. 2013). Kucharski et al. (2011) also analyzed with modification of Walker circulation. They showed that the Atlantic warming leads to rising motion and upper-level divergence in the African-Indian Ocean and sinking motion and upper-level convergence in the central-eastern Pacific. The sinking motion leads to low-level easterly anomalies in the central Pacific. Due to strong easterly anomalies, surface warm water moves to the west. Therefore, mean SST is getting cold due to effect of mean upwelling in the

eastern Pacific. Thus, mean SST over the eastern Pacific in the AMO run is relatively cold compared to that in the CNT run. The changes of mean climate in tropical Pacific caused by the AMO SST forcing are similar to results previously reported by Hong et al. (2013) and Kucharski et al. (2009).

The ENSO variability for the CNT run and the AMO run, analyzed in terms of the standard deviations of the SST anomalies over the tropical Pacific, are shown in Figs. 6a and 6b, respectively. The ENSO variability is clearly lower in the AMO run than in the CNT run. This result is consistent with those of previous studies based on observational data and other CGCMs (Dong et al. 2006; Timmermann et al. 2007; Kayano and Capistrano 2013). The zonal wind stress anomalies associated with ENSO were obtained by regressing the simulated Nino 3 index, which is the SST anomaly averaged over the region of 150°W - 90°W and 5°S - 5°N, on the zonal wind stress anomalies simulated over the tropical Pacific. The results for the CNT and AMO runs are shown in Figs. 7a and 7b. The most distinctive difference between the ENSO zonal wind stress anomalies of the AMO and CNT runs appears in the zonal location of maximum ENSO zonal wind stress anomalies. The location of the anomaly center in the AMO run is shifted to the west compared to that of the CNT run. The studies of Kang and Kug (2002) and Kim et al. (2011) indicated that the change in the

ENSO amplitude is related to the zonal shift of the zonal wind stress anomalies and that the thermocline anomalies in the tropical eastern Pacific during ENSO, which result in the SST changes, are also affected by the location of zonal wind stress anomalies. As seen in Fig. 8, the ENSO zonal wind stress anomalies in the AMO run are less effective at increasing the thermocline anomalies in the eastern Pacific compared to those in the CNT run. The westward shift of ENSO zonal wind stress anomalies in the AMO run results in smaller thermocline depth anomalies in the eastern Pacific, which lead to smaller SST variability in the eastern Pacific. Thus, the westward shift of the ENSO zonal wind stress anomalies appears to be a crucial factor in reducing the ENSO amplitude during the positive phase of the AMO. However, the question remains as to why the westward shift of the ENSO wind stress anomalies occurs in the positive phase of the AMO. In the next section, we will address this question with more concrete evidence on the important role of the westward shift of the wind stress anomalies on weakening the ENSO amplitude.

Table 1. List of experiments, model, and forcing used in this present study.

Experiments	Model	Forcing
CNT	SNU CGCM	Nudge with model climatological SST over the Atlantic
AMO		The same as CNT together with observed SST anomaly
CNT1	SNU AGCM	Prescribed with observed climatological SST
ENT1		The same as CNT1 together with El-Niño SST anomaly
CNT2		The same as CNT1 together with cold SST anomaly in the central pacific
ENT2		The same as CNT2 together with El-Niño SST anomaly
H-CNT	Hybrid coupled model	Prescribed with zonal wind stress anomalies of the CNT
H-AMO		Prescribed with zonal wind stress anomalies of the AMO

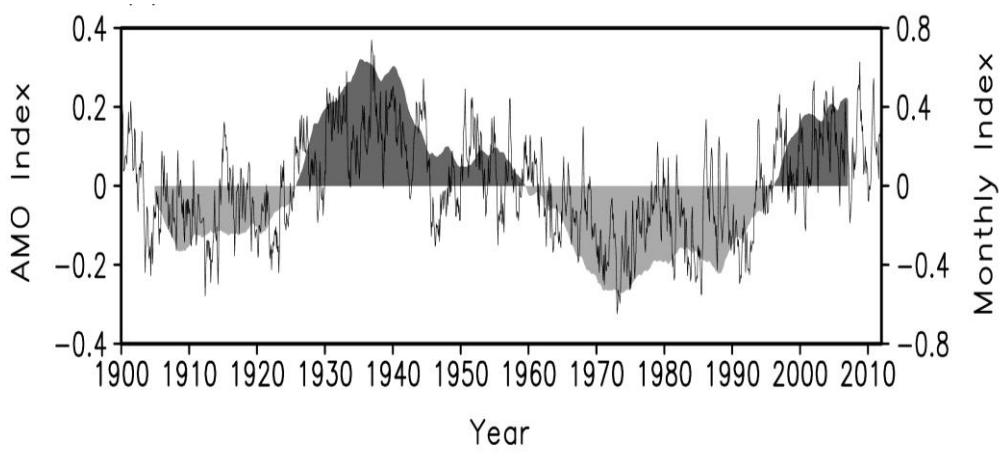

Figure. 1. Time series of the AMO index smoothed with a 121 month running mean (℃, shading) and its monthly index (℃, black solid line). The AMO index is obtained by the average of SST anomalies over the Northern Hemisphere Atlantic Ocean.

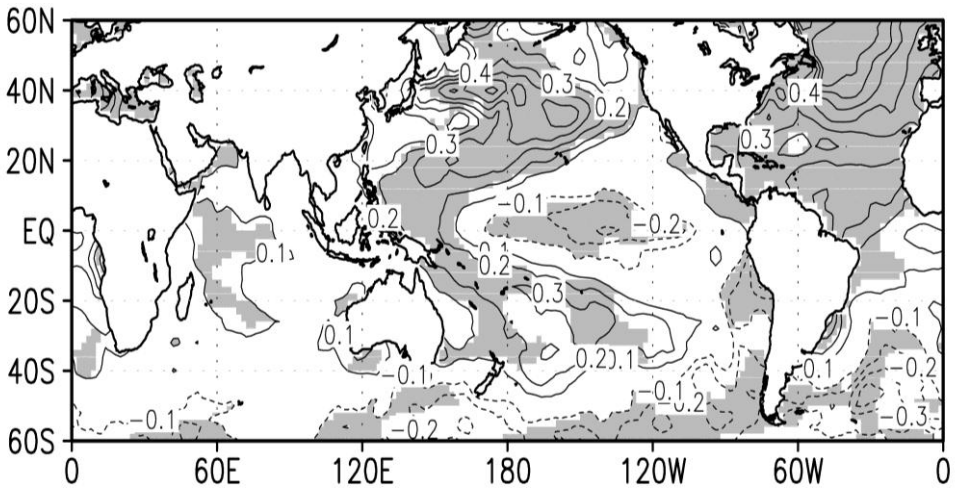

Figure. 2. Difference map between the mean SSTs during the positive phases of the AMO and those of the negative phases of the AMO. The differences with above 95% statistically significant level are indicated by shading.

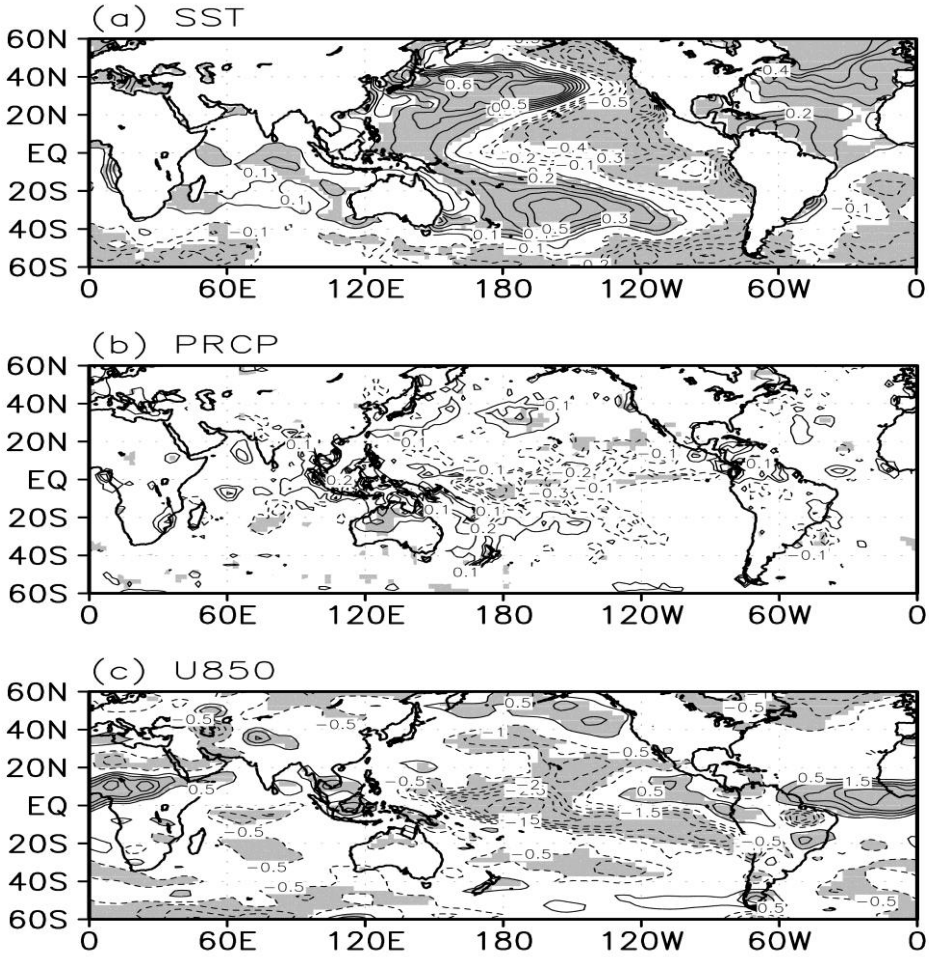

Figure. 3. Difference maps between the mean states for June 1998 - May 2013 and for June 1979 - May 1994. (a) SST (℃), (b) precipitation (mm day^{-1}), and (c) 850 hPa zonal wind (m s^{-1}). The differences with above 95% significant level are indicated by shading.

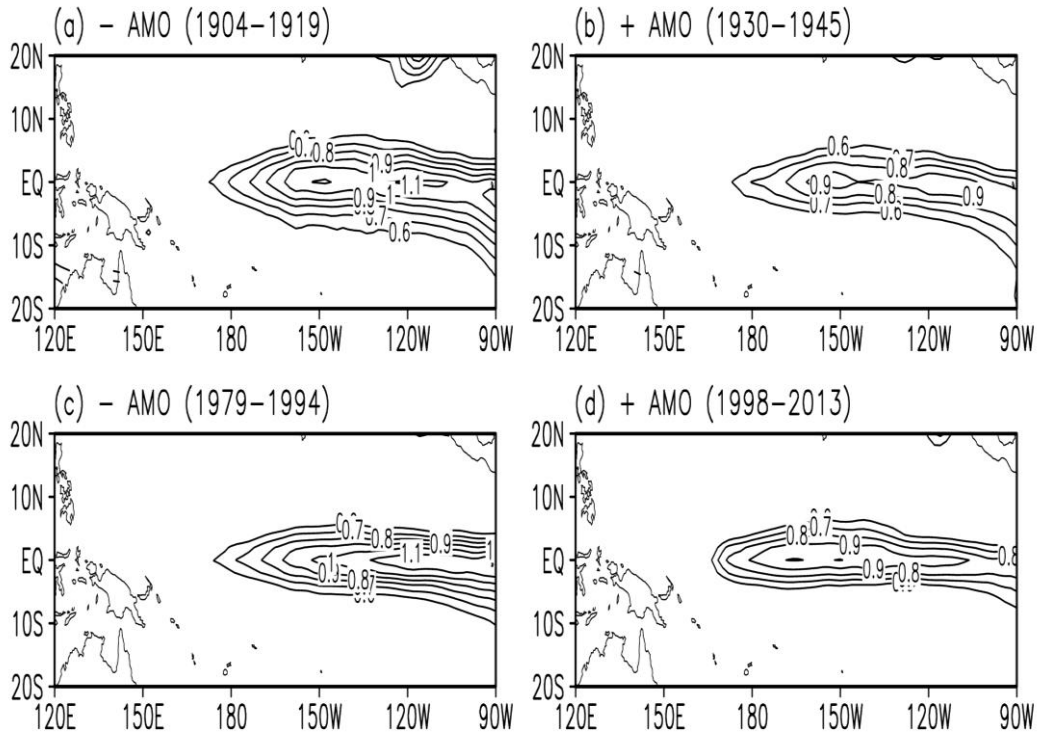

Figure. 4. Spatial patterns of the standard deviations of detrended SST anomalies over the tropical Pacific during the negative phase of the AMO of (a) 1904-1919 and (c) 1979-1994. (b) and (d) are in the positive phase of the AMO of 1930-1945 and 1998-2013, respectively.

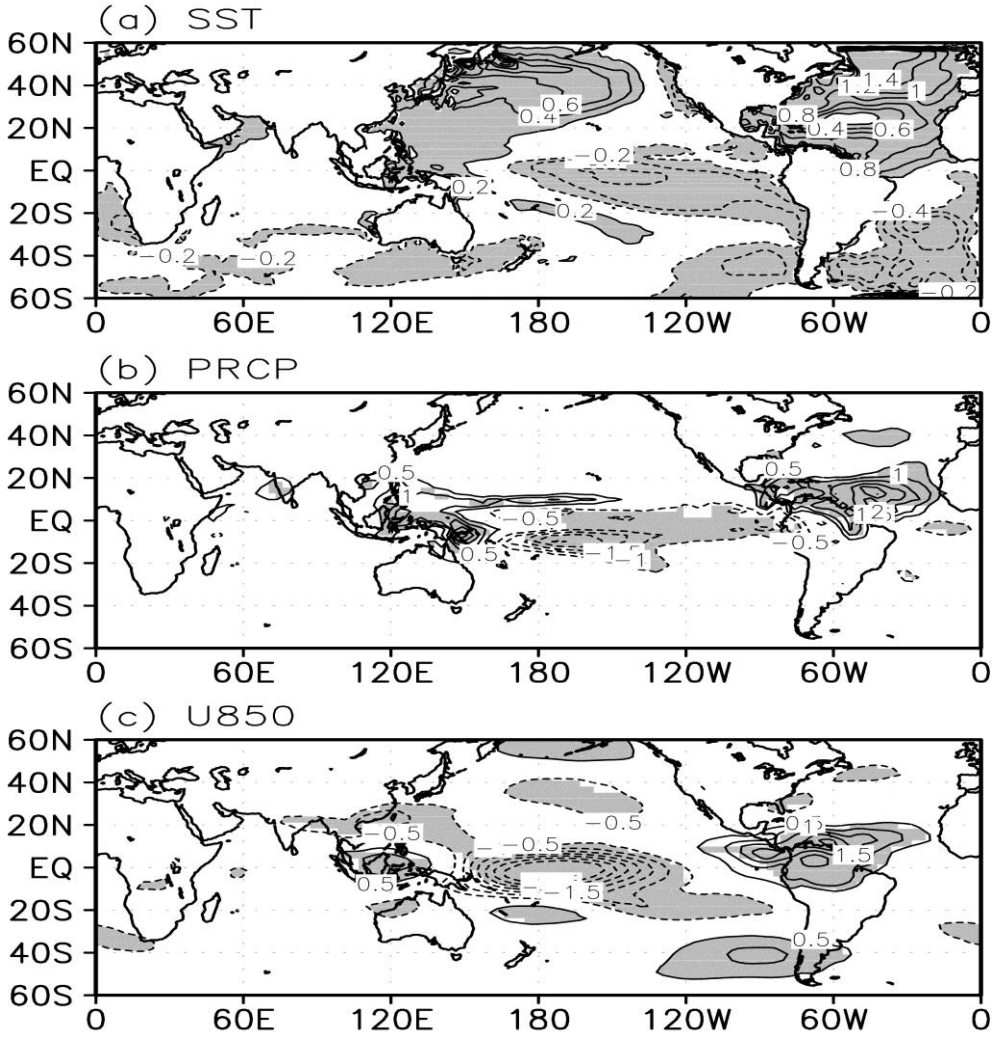

Figure. 5. Difference maps of (a) SST (℃), (b) precipitation (mm day^{-1}), and (c) 850 hPa zonal wind (m s^{-1}) between the CGCM experiments of the CNT and AMO runs. The differences with above 95% significant level are indicated by shading.

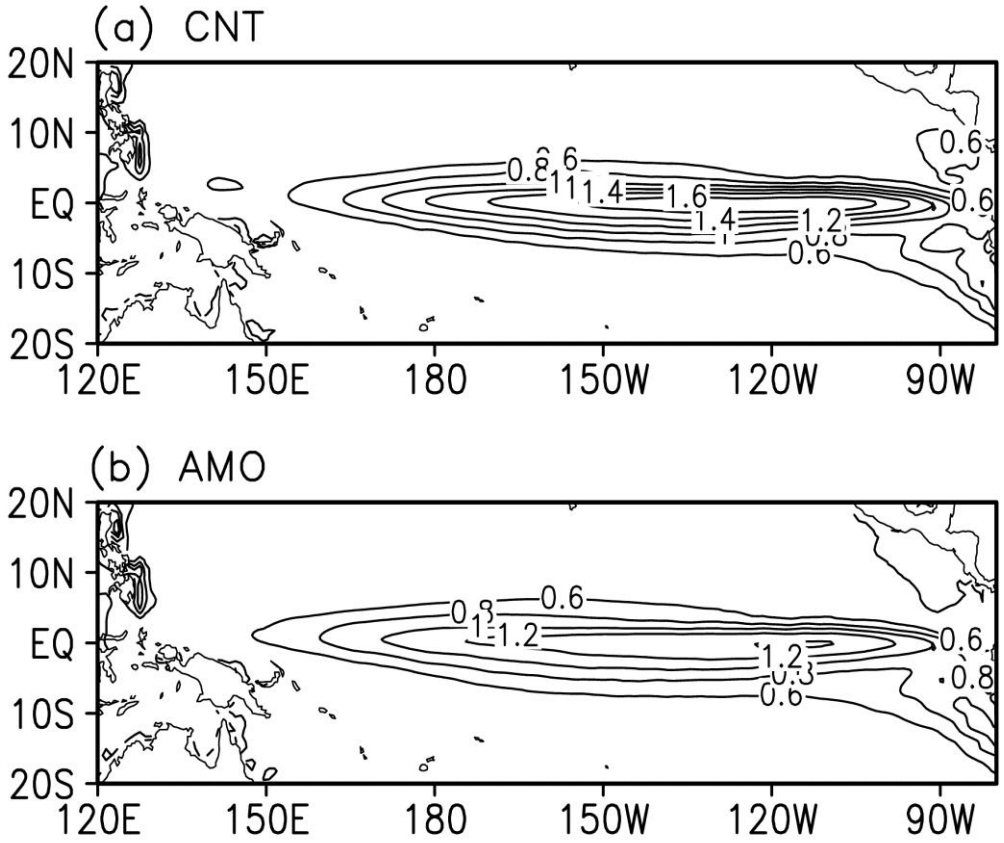

Figure. 6. Spatial patterns of the standard deviations of monthly SST anomalies (℃) over the tropical Pacific of (a) CNT and (b) AMO.

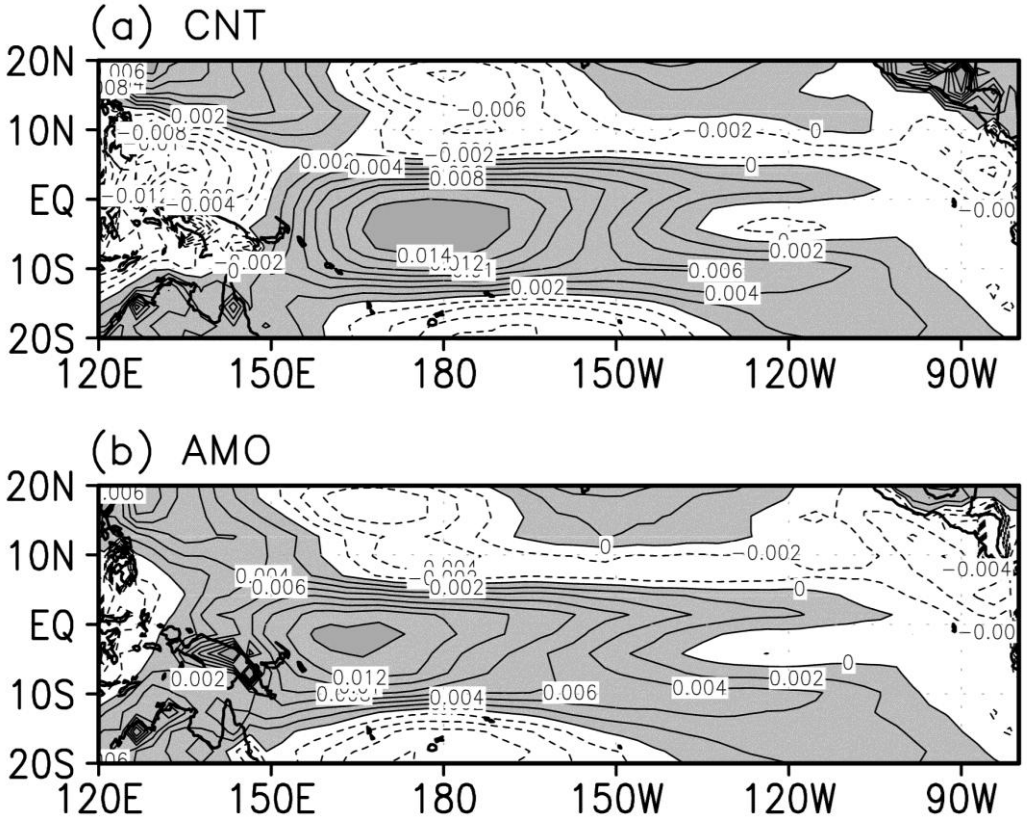

Figure. 7. Regression maps of the zonal wind stress anomalies in the tropical Pacific against the normalized Nino 3 index, obtained from the CGCM simulations for (a) CNT and (b) AMO. Unit is N m^{-2} $℃^{-1}$. Positive values are indicated by shading

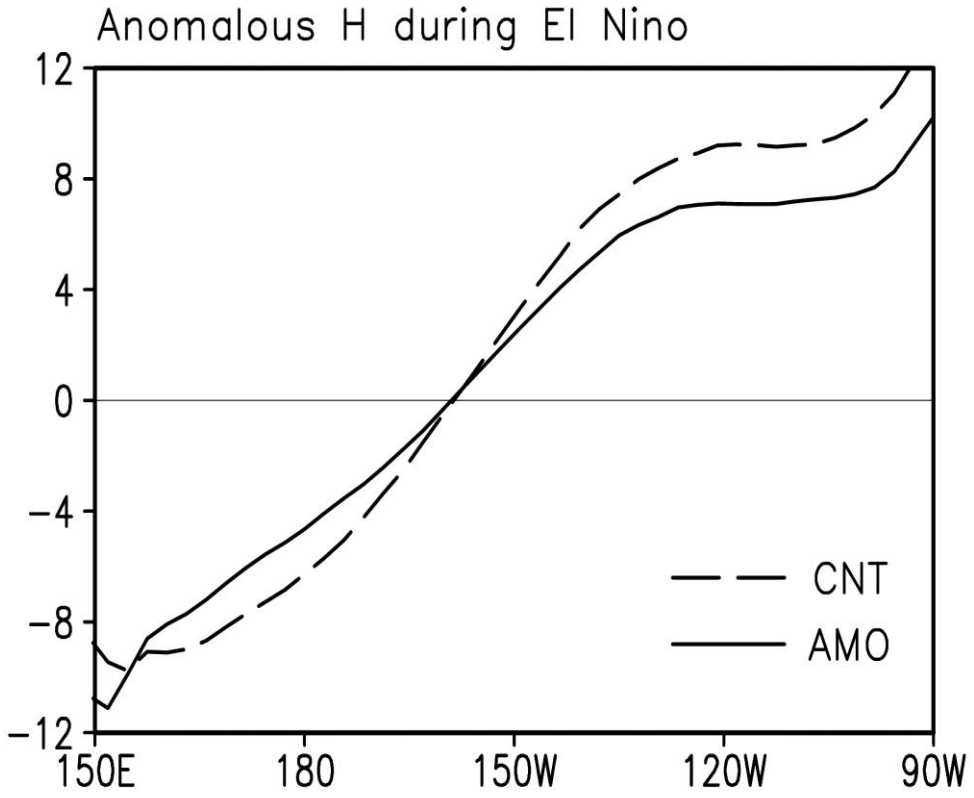

Figure. 8. Zonal structure of the thermocline depth anomalies (m) during the El Niño along the equator (5°S ~ 5°N) obtained by regressing the simulated Nino 3 index on the thermocline depth anomalies of the CNT (dashed line) and AMO (solid line) runs.

4. A mechanism for ENSO weakening in the positive phase of the AMO

In this study, we propose that the SST cooling in the central Pacific is responsible for the westward shift of the ENSO zonal wind stress anomalies during the positive phase of the AMO. To confirm this hypothesis, we performed two sets of AGCM experiments to investigate how different zonal wind stress anomalies respond to the same SST anomaly with different background mean SST states over the tropical Pacific. Two AGCM experiments in the first set are carried out with two different SSTs: one with the observed climatological SST (CNT1) and the other with the same climatological SST plus the El-Niño SST anomaly (ENT1) as shown in Fig. 9. The El-Niño SST anomaly during the averaged state of El-Niño for 1900-2013 is obtained from the first EOF of tropical Pacific SST anomalies. All experiments were integrated for 50 years and the last 30 years of data were used in the analysis. The zonal wind stress anomalies along the equator forced by the El-Niño SST anomaly under the observed climatological mean SST condition obtained by ENT1-CNT1 is indicated by the dashed line in Fig. 10. The second set of AGCM experiments (CNT2 and ENT2) is same as the first set except that the cold SST anomalies in

the central Pacific simulated by the AMO run, which are shown in the previous section, are included in the climatological mean SST. Thus, the difference between ENT2 and CNT2 provides the atmospheric anomalies forced by the same El-Niño SST anomaly as that of ENT1 but under the climatological tropical Pacific conditions influenced by the AMO. The zonal wind stress anomalies obtained by ENT2-CNT2 are indicated by the solid line in Fig. 10. The ENSO-related zonal wind stress anomalies under the climatological mean SST state during the positive phases of the AMO are shifted slightly to the west compared to anomalies without the slight cooling in the central Pacific, confirming that the slight cooling in the tropical central Pacific is responsible for the westward shift of the ENSO-related zonal wind stress anomalies in the tropical Pacific. This result can be interpreted as follows: the SST cooling located in the central pacific and the positive SST anomalies are less effective at increasing anomalous convection in the central Pacific (Kim et al. 2011; Chung and Li 2013). Thus, ENSO-related precipitation anomalies are shifted to the west toward the warm pool region compared to anomalies in other periods, and the zonal wind stress anomalies associated with the precipitation anomalies are also shifted to the west. It should be noted that the westward shift of the zonal wind stress anomalies is not as strong as in the simulation in the coupled model shown in

the previous section; this difference might be caused by a lack of ocean-atmosphere feedback in the present AGCM experiments.

The location change of the ENSO zonal wind stress anomalies can influence the ENSO amplitude, which was demonstrated by Kang and Kug (2002). Here, we assessed the impact of the westward shift of the ENSO zonal wind stress anomalies on the ENSO amplitude using a hybrid coupled model similar to that of Kang and Kug (2002), which was described in Section 2. The only difference between their model and the present model is the function of the wind stress anomaly, which is computed with the following formula

$$\tau\,(x, y, t) = \alpha\, F\,(x, y)\, T(t) \qquad (1)$$

where $T(t)$ is the model-produced Nino 3 SST anomaly in which the zonal wind stress anomalies are proportional to the Nino 3 SST anomaly; α is the scaling coefficient (which is 0.4 as used by Kang and Kug 2002); and $F(x, y)$ is the spatial function of the zonal wind stress anomalies. The spatial distributions of the wind stress functions are the same as those of Figs. 7a and 7b, which are the ENSO related zonal wind stress anomalies of the control and AMO coupled model experiments, respectively, described in the previous section. Two hybrid coupled model experiments, referred to as the H-CNT and H-AMO runs, were carried out with the two different zonal wind stress functions of Figs. 7a and 7b,

respectively. Both runs were integrated for 100 years and the model data produced for last 50 years were used for the following analysis. The time series of the Nino 3 SST anomaly produced by the hybrid coupled model are shown in Fig. 11. The dotted and solid lines indicate the H-CNT and H-AMO, respectively. The ENSO amplitude in the H-AMO run is clearly weaker than that of the H-CNT run. The standard deviation of the monthly Nino 3 SST index produced by the H-AMO run is decreased by 19% compared to that of the H-CNT run, confirming that the westward shift of the ENSO zonal wind stress anomalies plays a key role in weakening of the ENSO amplitude.

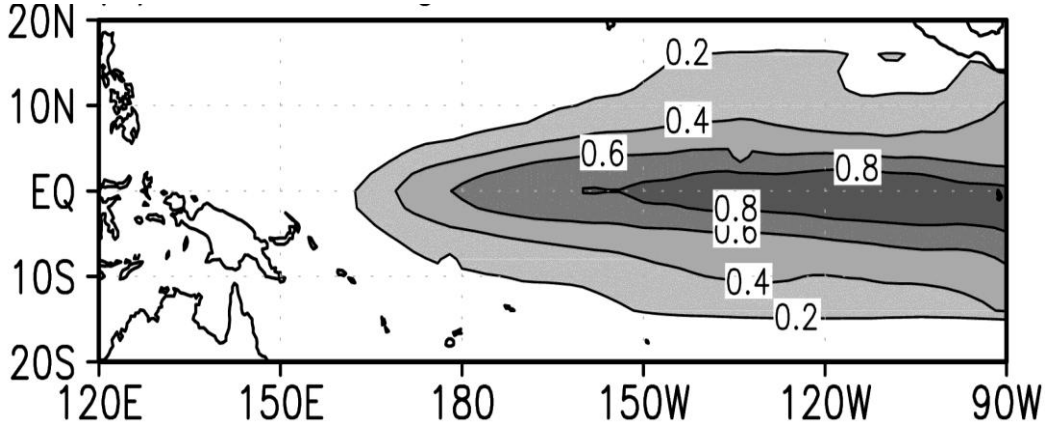

Figure. 9. The SST anomalies during the average state of El Niño's for 1900-2013, obtained from the first EOF of tropical Pacific SST anomalies.

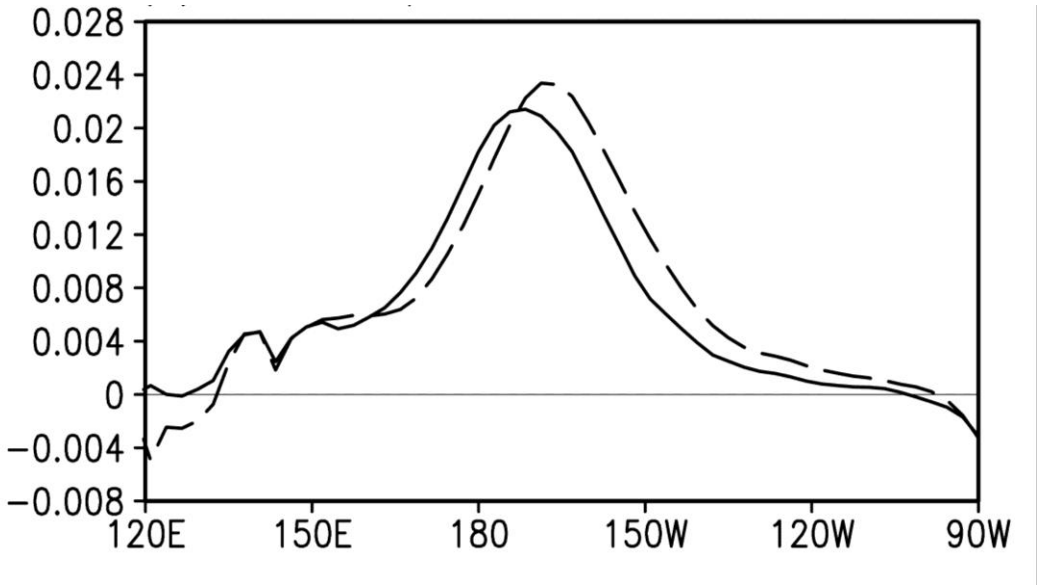

Figure. 10. The zonal wind stress anomalies ($\mathrm{N\,m^{-2}}$) along the equator (5°S ~ 5°N), simulated by an AGCM with two different SSTs prescribed. Two AGCM experiments were performed with the same SST anomalies shown in (a) in addition to the two different climatological SSTs. Dashed and solid lines indicate, respectively, for the observed climatological SST and for the same climatological SST plus the relatively cold SST anomalies over the central Pacific obtained by the SST difference between the CGCM experiments of the CNT and AMO runs. See the details in text.

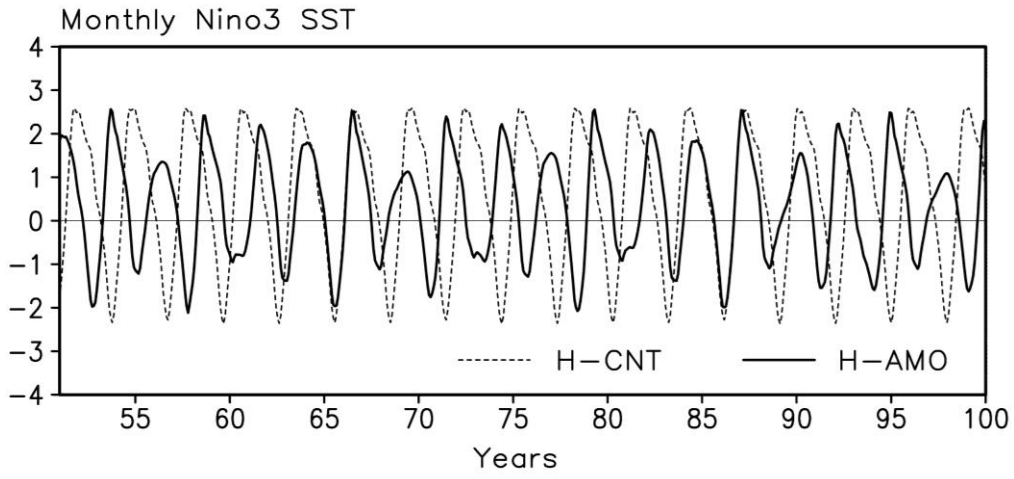

Figure. 11. Time series of Nino 3 SST anomalies simulated a hybrid coupled model with two different wind stress functions. Dotted and solid lines denote for the zonal wind stress functions whose spatial patterns are same as those of Figs. 6a and 6b, respectively.

5. Influence of the AMO on the warming and cooling center of SST anomaly associated with ENSO

In this chapter, we propose that the AMO is responsible for the occurrence of the Central Pacific (CP) El Niño events in recent decades. The different type of the El Niño is determined the location of the maximum SST anomaly. From this reason, we used Nino 3 index in winter (DJF) which ENSO peak period. Fig. 10 shows that scatterplot of the warming center and cooling center of SST anomalies against Nino 3 index in winter (DJF), separately. The black circle denotes the results in the CNT run and red circle denotes the result in the AMO run. It is difficult to classify the characteristics of the ENSO. We used criteria of maximum monthly SST anomaly center for determining the type of El Niño in Fig. 11. The Central Pacific (CP) El Niño region is defined as left black box (5°S - 5°N, 150°W - 180°) and Eastern Pacific (EP) El Niño region is defined as right black box (5°S - 5°N, 90°W - 120°). The other is Mixed El Niño region (5°S - 5°N, 12°W - 150°). Number of El Niño event stratified according to the center of maximum SST anomaly with Nino 3 index (Table 2). In the CNT run, El Niño occurred 35 times during 150 years. There is only Mixed (20times) and EP El Niño (15 times). The total number of El Niño event in the AMO run is same that

of the CNT. In the AMO run, however, CP El Niño occurred 10 times during 150 years. The number of CP El Niño event accounts for nearly 30 percent of the total El Niño event during 150 years. We confirm that impact of the AMO on the occurrence of the CP El Niño in the CGCM experiment. Recently, Xiang et al. (2013) has suggested that the central Pacific El Niño events will increase in the coming decades if the relatively cold mean SSTs persist over the central-eastern Pacific. The present study demonstrates that the SST cooling in the central Pacific occurred in recent decades is related to the warming of Northern Atlantic SST associated with a positive phase of the AMO and thus suggests that the frequent occurrence of the central Pacific El Niño may be related to the recent positive phase of the AMO.

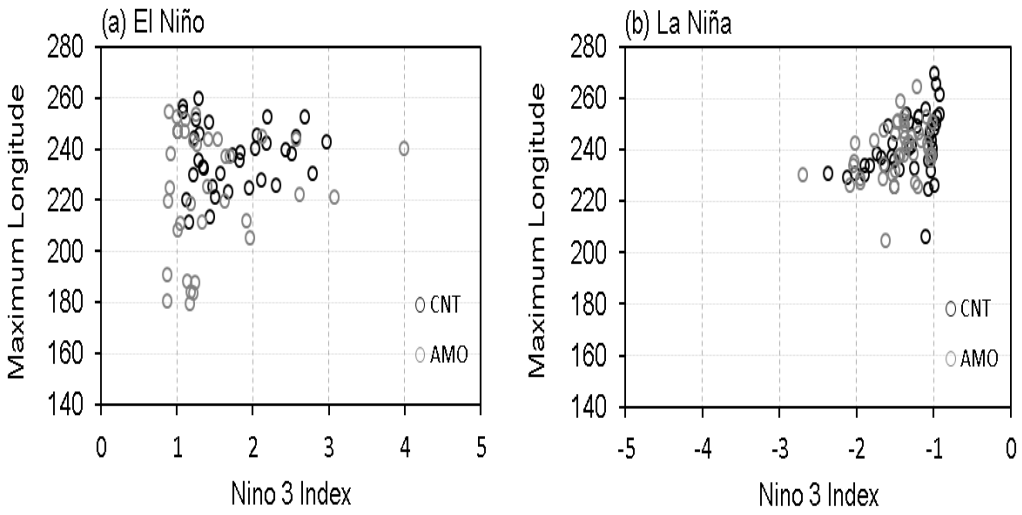

Figure 12. Scatterplot of (a) warming center of SST anomalies against Nino 3 index in winter(DJF) El Niño state and (b) cooling center of SST anomalies against Nino 3 index in winter (DJF) La Niña state from CNT (dark circle) and AMO (light circle) run.

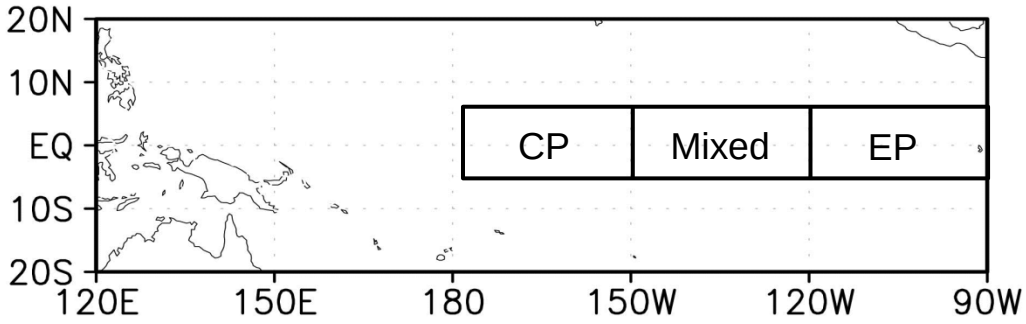

Figure 13. Black boxes are criteria of maximum monthly SST anomaly center for determining the type of El Niño. CP is defined as Central-Pacific El Niño (5°S - 5°N, 150°W - 180°) and EP is defined as Easter-Pacific El Niño (5°S - 5°N, 90°W - 120°). The other is Mixed El Niño (5°S - 5°N, 12°W - 150°).

Table 2. Frequency of El Niño year stratified according to SST anomaly warming center with Nino 3 index.

Experiment	CP El Niño	Mixed El Niño	EP El Niño
CNT	-	20 times (57%)	15 times (43%)
AMO	10 times (29%)	12 times (34%)	13 times (37%)

6. Discussion and conclusions

The mechanism for modulating the ENSO amplitude associated with the AMO was investigated using long-term observational data and CGCM experiments. Since the mid-1990s, the Atlantic Ocean has experienced warming in the Northern Hemisphere and the SST cooling has been observed together with the easterly wind anomalies in the tropical central Pacific. These observed anomalies in the Pacific are reproduced reasonably well by the CGCM experiment in which the Atlantic SSTs are nudged with those representing the positive phase of the AMO. The observational and coupled model experiments also show that the ENSO variability associated with the positive phase of AMO is weaker than the variability of other periods. These results are consistent with previous observational and model studies (Timmermann et al. 2007; Dong and Sutton 2007; Kayano and Capistrano 2013). Here, we further investigated the mechanism related to the weakening of the ENSO amplitude during the positive phase of the AMO.

The westward shift of the ENSO zonal wind anomalies in the tropical Pacific is a crucial factor for weakening of the ENSO variability during the positive phase of the AMO. The westward shift of the ENSO zonal wind stress anomalies

results from a slight cooling of the mean SSTs in the tropical central Pacific during the same period. The effect of the mean SST cooling could be interpreted as follows: with the relatively cold mean SST in the central pacific, the positive ENSO SST anomalies are less effective at producing anomalous convection in the central Pacific (Kim et al. 2011; Chung and Li 2013). Thus, the ENSO-related precipitation anomalies should be shifted to the west toward the warm pool region compared to those of other periods, and the zonal wind stress anomalies associated with the precipitation anomalies are also shifted to the west. The present study demonstrates that the westward shift of the zonal wind stress anomalies associated with ENSO results in a weakened the ENSO amplitude when a hybrid coupled model is used.

The westward shift of the zonal wind stress anomalies may also influence the period of ENSO and its decay. Based on the delayed oscillator mechanism (Suarez and Schopf 1988; Cane et al. 1990), the ENSO decay and the period of ENSO depend on westward-propagating Rossby waves. When the center of the zonal wind stress anomalies is shifted to the west, the distance for the Rossby waves to reach the western boundary is shortened (Kang and An 1998; An and Wang 2000). At the western boundary (WB), the Rossby waves are less damped because of a shorter distance of travel, so the reflected Rossby waves at the WB

can more effectively damp the pre-existing Kelvin waves in the eastern Pacific. This stronger negative feedback may underlie the weakening of the ENSO amplitude associated with the westward shift of the ENSO zonal wind stress anomalies and could provide an additional explanation as to why the ENSO amplitude does not increase effectively during the positive phase of the AMO.

The westward shift of the ENSO atmospheric anomalies could explain the frequent occurrence of the central Pacific El Niño events in recent decades (Xiang et al. 2013; Chung and Li 2013). The mean SST cooling in the central Pacific could be an important cause for the westward shift of the ENSO atmospheric anomalies. Xiang et al. (2013) has suggested that the central Pacific El Niño events will increase in the coming decades if the relatively cold mean SSTs persist over the central-eastern Pacific. The present study demonstrates that the SST cooling in the central Pacific occurred in recent decades is related to the warming of Northern Atlantic SST associated with a positive phase of the AMO and thus suggests that the frequent occurrence of the central Pacific El Niño may be related to the recent positive phase of the AMO.

The implication of the present results can be extended to explain the climate shift that occurred in the end of the 20th century in the Pacific region. As mentioned above, the observed decadal change from 1980s to 2000s is well

reproduced not only in the Atlantic but also the other region by the model with the AMO SST forcing. A recent studies have suggested different possible mechanism to explain the climate shift over the Pacific (Chung and Li 2013; Farneti et al. 2013). Chung and Li (2013) pointed out that the mean state over the equatorial Pacific undergoes a regime change according to the phase transition of the Pacific decadal oscillation (PDO), which also shows a transition from a warm phase to a cold phase around 1999. Similar to previous study, Farneti et al. (2013) suggested that the Pacific interdecadal variability is driven by interactions between the tropical Pacific and the extratropical Pacific with atmospheric and oceanic bridge. Further studies are needed to investigate what is the most important factor for climate shift over the Pacific in recent decades.

Acknowledgments. This work was supported by the National Research Foundation of Korea Grant funded by the Korean Government (MEST) (NRF-2012M1A2A2671775) and by the Brain Korea 21 Plus Project.

References

Adler, R. F., and Coauthors, 2003: The version-2 global precipitation climatology project (GPCP) monthly precipitation analysis (1979-present). *J Hydrometeorol*, **4,** 1147-1167.

An, S. I., and B. Wang, 2000: Interdecadal change of the structure of the ENSO mode and its impact on the ENSO frequency. *J Climate*, **13,** 2044-2055.

Bonan G. B., 1996: A land surface model (LSM version 1.0) for ecological, hydrological, and atmospheric studies: technical description and user's guide. NCAR Techical Note NCAR/TN417 + STR, National Center For Atmospheric Research Boulder, Colorado, 50 pp.

Cane, M. A., and S. E. Zebiak, 1987: Prediction of El Niño events using a physical model, in Atmosphere and Ocean Variability, edited by H. Cattel, R. Meteorol. Soc. Press, London, 183 pp.

Cane, M. A., M. Munnich, and S. E. Zebiak, 1990: A Study of Self-Excited Oscillations of the Tropical Ocean - Atmosphere System .1. Linear-Analysis. *Journal of the Atmospheric Sciences*, **47,** 1562-1577.

Chung, P. H., and T. Li, 2013: Interdecadal relationship between the mean state and El Nino types. *J Climate*, **26,** 361-379.

Delworth, T. L., and M. E. Mann, 2000: Observed and simulated multidecadal variability in the Northern Hemisphere. *Climate Dynamics*, **16,** 661-676.

Ding, H., N. S. Keenlyside, and M. Latif, 2012: Impact of the Equatorial Atlantic on the El Nio Southern Oscillation. *Climate Dynamics*, **38,** 1965-1972.

Dong, B. W., R. T. Sutton, and A. A. Scaife, 2006: Multidecadal modulation of El Nino-Southern Oscillation (ENSO) variance by Atlantic Ocean sea surface temperatures. *Geophys Res Lett*, **33**, L08705, doi:10.1029/2006GL025766.

Dong, B., and R. T. Sutton, 2007: Enhancement of ENSO variability by a weakened Atlantic thermohaline circulation in a coupled GCM. *J Climate*, **20,** 4920-4939.

Enfield, D. B., A. M. Mestas-Nunez, and P. J. Trimble, 2001: The Atlantic multidecadal oscillation and its relation to rainfall and river flows in the continental US. *Geophys Res Lett*, **28,** 2077-2080.

Ham, Y. G., I. S. Kang, D. Kim, and J. S. Kug, 2012: El-Nino Southern Oscillation simulated and predicted in SNU coupled GCMs. *Climate Dynamics*, **38,** 2227-2242.

Holtslag, A. A. M., and B. A. Boville, 1993: Local Versus Nonlocal Boundary-Layer Diffusion in a Global Climate Model. *J Climate*, **6,** 1825-1842.

Hong, S., I. S. Kang, I. Choi, and Y. G. Ham, 2013: Climate responses in the

tropical pacific associated with atlantic warming in recent decades. *Asia-Pac J Atmos Sci*, **49,** 209-217.

Kalnay, E., and Coauthors, 1996: The NCEP/NCAR 40-year reanalysis project. *B Am Meteorol Soc*, **77,** 437-471.

Kang, I. S., and S. I. An, 1998: Kelvin and Rossby wave contributions to the SST oscillation of ENSO. *J Climate*, **11,** 2461-2469.

Kang, I. S., and J. S. Kug, 2000: An El-Nino prediction system using an intermediate ocean and a statistical atmosphere. *Geophys Res Lett*, **27,** 1167-1170.

Kang, I. S., and J. S. Kug, 2002: El Nino and La Nina sea surface temperature anomalies: Asymmetry characteristics associated with their wind stress anomalies. *J Geophys Res-Atmos*, **107**, 4372, doi:10.1029/2001JD000393.

Kayano, M. T., and Capistrano, V. B., 2013: How the Atlantic multidecadal oscillation (AMO) modifies the ENSO influence on the South American rainfall. *Int J Climatol*, doi:10.1002/joc.3674.

Keenlyside, N. S., H. Ding, and M. Latif, 2013: Potential of equatorial Atlantic variability to enhance El Niño prediction. *Geophys Res Lett*, 40, 2278-2283.

Kerr, R. A., 2000: A North Atlantic climate pacemaker for the centuries. *Science*, 288, 1984-1986.

Kim, D., J. S. Kug, I. S. Kang, F. F. Jin, and A. T. Wittenberg, 2008: Tropical Pacific impacts of convective momentum transport in the SNU coupled GCM. *Climate Dynamics*, **31,** 213-226.

Kim, D., Y. S. Jang, D. H. Kim, Y. H. Kim, M. Watanabe, F. F. Jin, and J. S. Kug, 2011: El Nino-Southern Oscillation sensitivity to cumulus entrainment in a coupled general circulation model. *J Geophys Res-Atmos*, **116**, doi:10.1029/2011JD016526.

Knight, J. R., R. J. Allan, C. K. Folland, M. Vellinga, and M. E. Mann, 2005: A signature of persistent natural thermohaline circulation cycles in observed climate. *Geophys Res Lett*, **32,** doi:10.1029/2005GL024233.

Kug, J. S., J. Y. Lee, I. S. Kang, B. Wang, and C. K. Park, 2008: Optimal Multi-model Ensemble Method in Seasonal Climate Prediction. *Asia-Pac J Atmos Sci*, **44,** 259-267.

Lee, M. I., I. S. Kang, J. K. Kim, and B. E. Mapes, 2001: Influence of cloud-radiation interaction on simulating tropical intraseasonal oscillation with an atmospheric general circulation model. *J Geophys Res-Atmos*, **106,** 14219-14233.

Lee, M. I., I. S. Kang, and B. E. Mapes, 2003: Impacts of cumulus convection parameterization on aqua-planet AGCM Simulations of tropical

intraseasonal variability. *J Meteorol Soc Jpn*, **81,** 963-992.

Nakajima T, Tsukamoto, Y. Tsushima, and A. Numaguti, 1995: Modelling of the radiative processes in an AGCM. *Climate system dynamics and modelling*, **3**, 104-123.

Noh, Y., and H. J. Kim, 1999: Simulations of temperature and turbulence structure of the oceanic boundary layer with the improved near-surface process. *J Geophys Res-Oceans*, **104,** 15621-15634.

Numaguti, A., M. Takahasi, T. Nakajima, and A. Sum, 1995: Development of an atmospheric general circulation model. *Climate System Dynamics and Modelling*, **3**, 1-27.

Rodriguez-Fonseca, B., I. Polo, J. Garcia-Serrano, T. Losada, E. Mohino, C. R. Mechoso, and F. Kucharski, 2009: Are Atlantic Ninos enhancing Pacific ENSO events in recent decades? *Geophys Res Lett*, **36**, doi: 10.1029/2009GL040048.

Smith, T. M., R. W. Reynolds, T. C. Peterson, and J. Lawrimore, 2008: Improvements to NOAA's historical merged land-ocean surface temperature analysis (1880-2006). *J Climate*, **21,** 2283-2296.

Suarez, M. J., and P. S. Schopf, 1988: A Delayed Action Oscillator for Enso. *Journal of the Atmospheric Sciences*, **45,** 3283-3287.

Sutton, R. T., and D. L. R. Hodson, 2005: Atlantic Ocean forcing of North American and European summer climate. *Science*, **309,** 115-118.

Timmermann, A., and Coauthors, 2007: The influence of a weakening of the Atlantic meridional overturning circulation on ENSO. *J Climate*, **20,** 4899-4919.

Wang, C. Z., S. F. Dong, and E. Munoz, 2010: Seawater density variations in the North Atlantic and the Atlantic meridional overturning circulation. *Climate Dynamics*, **34,** 953-968.

Xiang, B. Q., B. Wang, and T. Li, 2013: A new paradigm for the predominance of standing Central Pacific Warming after the late 1990s. *Climate Dynamics*, **41,** 327-340.

Yeh, S. W., and B. P. Kirtman, 2005: Pacific decadal variability and decadal ENSO amplitude modulation. *Geophys Res Lett*, **32**, doi: 10.1029/2004GL021731.

Zhang, R., and T. L. Delworth, 2007: Impact of the Atlantic Multidecadal Oscillation on North Pacific climate variability. *Geophys Res Lett*, **34**, doi: 10.1029/2007GL031601.

국 문 초 록

본 연구에서는 대서양 장주기 변동이 엘니뇨 남방진동을 조절하는 매커니즘에 대하여 관측 자료와 대기 해양 접합 모형을 이용한 연구를 수행하였다. 대서양 장주기 변동이 양의 상태일때는 엘니뇨 남방진동의 크기가 약해지고, 음의 상태일때는 크기가 증가하는 관계를 1900 년부터 2013 년까지의 관측 자료를 통해 확인 할 수 있다. 최근 15 년간 엘니뇨 남방진동의 약화는 태평양의 평균 기후장의 변화와 연관되어 있다. 특히, 동태평양의 차가운 해수면 온도와 열대태평양의 동풍 아노말리가 연관되어 있다. 대서양 해수면 온도를 양의 상태의 대서양 장주기 변동을 나타내는 온도 패턴으로 강제된 대기 해양 접합 모델 실험을 통하여 관측에서 나타나는 특징들을 재현하였다. 대서양 장주기 변동이 양의 상태일 때 엘니뇨 동서바람응력 아노말리가 서쪽으로 이동한 것이 엘니뇨 남방진동의 크기로 이어진다는 매커니즘이 중간단계 대기 해양 접합 모형을 통하여 확인 되었다. 엘니뇨 동서바람응력 아노말리가 서쪽으로 이동하는 것은 강수 아노말리가 서쪽으로 이동하기 때문이다. 이러한 강수 아노말리의 이동은 대서양 장주기 변동이 양의 상태일 때 나타나는 중태평양의 차가운 배경 해수면 온도와 연관되어 있다. 그러므로 본 연구에서는 대서양 장주기 변동이 열대 태평양의 배경장을 변화시킴으로 이것을 통한 엘니뇨 남방진동의 크기를 조절하는데 중요한 역할을 한다는 것을 설명하였다.

주요어: 바람응력의 서쪽이동, 대서양 장주기 변동, 기후 변화, 자연 변동성, 엘니뇨 남방 진동

학생번호: 2012-20338